Electronic Supplementary Material

Harnessing Thermal Waste with a Poling-free Molecular Pyroelectric Zinc(II) Complex

Rajashi Haldar, [a] Sudip Naskar, [b] Bapan Jana,[a] Dipankar Mandal,[b] * Maheswaran Shanmugam[a,] *

[a] Rajashi Haldar, Bapan Jana, Maheswaran Shanmugam
Department of Chemistry,
Indian Institute of Technology Bombay,
Powai, Mumbai-400076, Maharashtra, India
E-mail: eswar@chem.iitb.ac.in

[b] Sudip Naskar, Dipankar Mandal
Quantum Materials and Devices Unit,
Institute of Nano Science and Technology Mohali
Knowledge City, Sector 81, Mohali 140306, India
E-mail: dmandal@inst.ac.in

Experimental section:

Materials and Methods: All of the chemical reagents in the synthesis were of reagent grade and used without further purification.

Single crystal X-ray diffraction measurement: The single-crystal diffraction data of the complex was collected on a Bruker diffractometer with Mo Kα radiation (λ = 0.71073 Å). Data reduction and the unit cell parameters were determined by using CrysAlisPro 1.171.38.43. With the help of Olex2 software with the SHELXL program, crystal data was solved by direct method and refined by the least square procedure. All non-hydrogen atoms were refined anisotropically and the positions of all hydrogen atoms were generated geometrically. The data collection and structure refinement of these crystals are summarized in Table S1. **Powder X-ray diffraction (PXRD):** Powder XRD measurements were carried out in a Rigaku D/tex Ultra 250 instrument, using Cu K_β filter with a scan speed of 5° /min at room temperature and at variable temperatures. Diffraction patterns were collected in the 2θ range of 5–50° with a step size of 0.01°. **Hirshfeld surface analysis:** The Hirshfeld surface mapping of all the non-covalent molecular interactions of complex **1** was done using the Crystal Explorer 3.1 program. The single-crystal X-ray crystallographic information file (CIF) was utilized to visualize all the different type of interactions which are present on the Hirshfeld surface. These interactions were obtained as 3D color mapping images such as normalized contact distance (dnorm), shape index and curvedness. The diverse surface colour mappings were generated on the Hirshfeld surface by various colour coding based on strong (red), medium (blue) and weak (white) interactions. **Thermal analyses**: Differential scanning calorimetry (DSC) was done using a Rigaku DSC Vesta instrument by heating and cooling crystalline samples with a rate of 5 K min^{-1} in aluminium crucibles at nitrogen atmosphere. Thermogravimetric analyses (TGA) were carried out on a Rigaku TGMS-ThemoMass Photo instrument by heating crystalline samples with a rate of 5 K/min under nitrogen atmosphere. **Dielectric measurement:** Complex dielectric permittivity was measured with Keysight Impedance Analyzer E4990A system, where two parallel plate capacitor geometry is considered. Silver conductive paste deposited on both sides of the pressed pellets of the sample were used as top and bottom electrodes.

Ferroelectric measurement: Ferroelectric measurements were also performed on pressed pellets using a Radiant Precision Multiferroic II ferroelectric loop tracer with high voltage amplifier (EEL 1102.05.2, Electrical Energy Limited). A voltage waveform is applied to the sample in a series of voltage steps. At each voltage step, the current induced in the sample by

the voltage step is integrated and the integral value is captured and converted into Polarization ($\mu C/cm^2$) by:

$$\frac{\mu C}{cm^2} = \frac{Q}{Area} = \frac{CV}{Area} = \frac{Sense\ Capacitor\ \times\ Integrator\ Volts}{Sample\ Area} \quad (1)$$

(1) is scaled by appropriate factors to properly adjust computed values to the standard polarization units of $\mu C/cm^2$.

The voltage waveform is a standard bipolar triangular waveform that can be simply defined by providing the maximum voltage and the entire duration of the waveform in milliseconds. The sign of the voltage indicates the direction of the first leg of the waveform. The number of points are controlled primarily by the duration of the waveform, though it may also be adjusted by the voltage. The waveform begins at zero volts and steps to a maximum value of the assigned voltage. It then proceeds to step to the negative side of the assigned maximum, and finally steps back to zero volts. The measurements are done by applying the voltage for a time period of 20 ms.

Pyroelectric measurement:

A pressed pellet (diameter ~ 10 mm, thickness~0.65 mm) with silver top and bottom electrodes (diameter ~ 5.2 mm area~ 22.05 mm^2) is used to harvest thermal energy harvesting. Pyroelectric measurements were performed by in-house customised setup, where infra-red lamp (heat source) was used with function generator and chopper circuit to control the heating and cooling of the crystal. The temporal change in temperature was measured with thermocouple and pyroelectric current was recorded by using Keithley SMU 2450.

PFM measurement: Local topography, piezoelectric properties and ferroelectric switching were studied on a pressed pellet by scanning probe microscopy (SPM) technique using piezo-response force microscopy (PFM) in DART (Dual AC Resonance Tracking) mode, in a MFP-3D BIO instrument (Asylum Research) using an SCM-PIT-V2 probe. The amplitude and phase images were recorded by applying fixed ac voltage and the typical butterfly loops and phase loops were recorded by applying different DC biases to tip with the AC voltage.

By the definition of the converse piezoelectric effect, the piezoelectric coefficient (d_{33}) magnitude can be calculated from the equation, $d_{33} = \Delta z/V$; where Δz is the displacement of the

tip caused by the deformation of ferroelectric samples under applied electric field and V is the applied voltage. Δz can be calculated from the slope of the linear part of the amplitude vs. voltage curve (butterfly loop) (Jalalian et al., *Appl. Phys. Lett.* 2014, **104**, 103112).

Synthetic procedure for 1:

To an aqueous solution of $ZnSO_4.7H_2O$ (0.287 g, 1 mmol), 2,2′-bipyridine (0.156 g, 1 mmol) dissolved in 10 mL of ethanol was added. The solution was refluxed for 2 hours at 80°C. After 2 hours, aqueous solution of $NaClO_4$ (0.184 g, 1.5 mmol) was added into the reaction mixture and it was cooled down to room temperature. The resultant reaction mixture was filtered and the filtrate was kept for crystallization at room temperature. Block shaped pale pink coloured single crystals were grown from filtrate after four to five days which were suitable for single crystal X-ray diffraction. Yield of **1**: 0.19 g (68%). Elemental composition of **1** Calc. (%): C, 49.19; H, 3.30; N, 11.46. Found (%): C, 49.16; H, 3.32; N, 11.40.

Scheme S1: Synthetic scheme followed to isolate **1.**

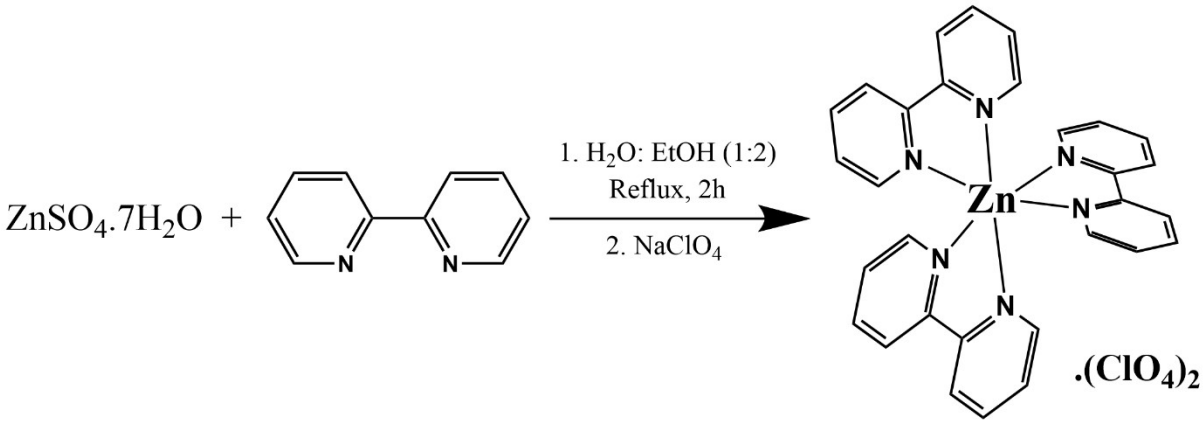

Table S1. Crystallographic parameters for complex **1.**

Parameter	**1**	**1a**	**1b**
Empirical formula	$C_{30}H_{26}Cl_2N_6O_9Zn$	$C_{30}H_{24}Cl_2N_6O_8Zn$	$C_{30}H_{24}Cl_2N_6O_8Zn$
Formula weight	750.84	732.82	732.82
Crystal system	monoclinic	monoclinic	trigonal
Space group	C2	C2/c	$P\bar{3}c$
a/Å	22.9073(8)	17.5478(6)	10.5944(9)
b/Å	14.4467(4)	10.8370(4)	10.5944(9)
c/Å	21.7890(7)	16.1007(5)	16.2218(14)
α/°	90	90	90
β/°	114.642(4)	91.106(3)	90
γ/°	90	90	120
Volume/$Å^3$	6554.1(4)	3061.23(18)	1576.8(3)
Z	8	4	2
$\rho_{calc}g/cm^3$	1.485	1.590	1.611
μ/mm^{-1}	0.971	1.039	1.017
F(000)	2992.0	1496.0	780.0
Crystal size/mm^3	0.183 × 0.156 × 0.098	0.183 × 0.156 × 0.098	0.183 × 0.156 × 0.098
Temperature/K	300.0(10)	340.0(10)	390.0(10)
$2\Theta_{max}$	50	50	50
Radiation	Mo Kα	Mo Kα	Mo Kα
λ [Å]	0.71073	0.71073	0.71073
Reflns	103799	25950	18182
Ind. reflns	11534	2688	935
Goodness-of-fit on F^2	1.042	1.034	1.084
R_1	0.0833	0.0533	0.0966
wR_2	0.2264	0.1340	0.2607

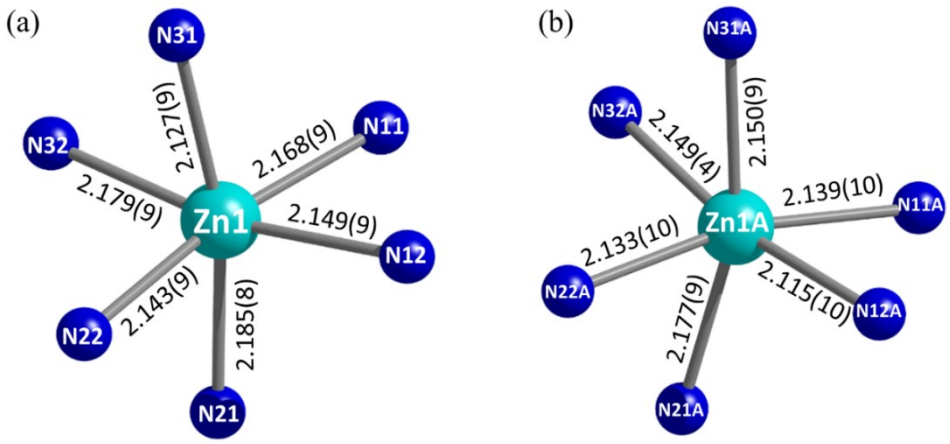

Figure S1. Selected bond lengths for two crystallographically independent molecules (a and b) present in the asymmetric unit of complex **1**.

Table S2: Selected bond angles for complex **1.**

Bond Angle	Value (°)	Bond Angle	Value (°)
∠N11-Zn1-N12	76.5(4)	∠N11A-Zn1A-N12A	75.8(4)
∠N11-Zn1-N21	93.8(4)	∠N11A-Zn1A-N21A	94.5(3)
∠N11-Zn1-N22	96.2(4)	∠N11A-Zn1A-N22A	94.4(4)
∠N12-Zn1-N22	171.3(4)	∠N12A-Zn1A-N22A	166.4(4)
∠N21-Zn1-N31	167.1(4)	∠N21A-Zn1A-N31A	163.5(3)
∠N21-Zn1-N12	99.1(4)	∠N21A-Zn1A-N12A	95.1(3)
∠N21-Zn1-N32	95.2(4)	∠N21A-Zn1A-N32A	93.5(3)
∠N21-Zn1-N22	76.4(4)	∠N21A-Zn1A-N22A	76.0(3)
∠N31-Zn1-N11	94.8(4)	∠N31A-Zn1A-N11A	97.5(3)
∠N31-Zn1-N12	92.3(3)	∠N31A-Zn1A-N12A	98.7(3)
∠N31-Zn1-N22	93.0(4)	∠N31A-Zn1A-N22A	91.9(3)
∠N32-Zn1-N11	168.5(4)	∠N32A-Zn1A-N11A	170.3(3)
∠N32-Zn1-N12	95.0(3)	∠N32A-Zn1A-N12A	98.2(4)
∠N32-Zn1-N22	92.8(4)	∠N32A-Zn1A-N22A	92.7(3)
∠N32-Zn1-N31	77.6(4)	∠N32A-Zn1A-N31A	75.7(3)

Table S3: Atoms involved in intermolecular hydrogen bonding and its corresponding bond distances and bond angles in complex **1**.

H-Bond Donor(D)- Acceptor(A)	D….A (Å)	∠DHA (°)
C21A-H21A...O24_$1	3.27(3)	143.4
C34A-H34A...O21A_$1	3.33(4)	136.0
C40A-H40A...O14_$2	3.15(2)	145.3
C17-H17...O12_$3	3.41(2)	123.4
C31-H31...O14A_$4	3.326(19)	118.8
C29-H29...O13A_$4	3.34(3)	114.7
C30-H30...O13A_$4	3.22(3)	124.7
C30-H30...O14A_$4	3.48(2)	119.9
C12A-H12A...O12_$5	3.47(2)	161.9
C27-H27...O1S_$6	3.31(3)	150.3
O1S-H1SA...O23_$6	2.95(7)	143.1
C28A-H28A...O24A_$7	3.30(3)	119.4
C27A-H27A...O24A_$7	3.39(3)	110.6
C20-H20...O24A_$8	3.32(3)	116.7
C13A-H13A...O23A_$8	3.24(3)	122.9
C14A-H14A...O23A_$8	3.40(3)	111.4
C20-H20...O22_$9	3.08(2)	113.8
C37A-H37A...O21A_$9	3.36(4)	138.2
C19A-H19A...O11A_$10	3.324(17)	132.4
C12-H12...O11	3.31(2)	122.1
C12-H12...O12_$11	3.36(2)	113.7
C23-H23...O21	3.25(2)	130.6
C13-H13...O11	3.28(2)	123.5
C31-H31...N11	3.282(18)	118.3
C21-H21...N12	3.423(16)	119.6
C31A-H31A...N11A	3.358(16)	122.0
C31A-H31A...O11A	3.274(17)	127.7
C20A-H20A...N32A	3.393(16)	120.5
C21A-H21A...N12A	3.272(15)	119.6
C11A-H11A...O12A	3.36(2)	130.2
C11A-H11A...N22A	3.307(17)	118.3

$1 = -x+1.5, y-0.5, -z; $2= -x+2, y, -z+1; $3 = -x+2, y, -z; $4 = -x+1.5, y+0.5, -z; $5 = x-0.5, y-0.5, z; $6 = x, y+1, z; $7= -x+1, y, -z; $8 = x+1, y-1, z-1; $9 = -x+1, y, -z+1; $10 = -x+1.5, y+0.5, -z+1; $11 = -x+1.5, y-0.5, -z+1;

Figure S2. Packing diagram of **1**. Orange dotted lines represent O…H hydrogen bonding with O atom of water molecule and C-H bond as well as between H atom of the water molecule and O atom of Cl-O bond. Magenta dotted lines represent O…H hydrogen bonding between H atom of C-H bond and O atom of ClO_4 anion. Colour Code: Zinc: cyan; Carbon: dark grey; Nitrogen: blue; Oxygen: Red; Chlorine: green; Hydrogen: black.

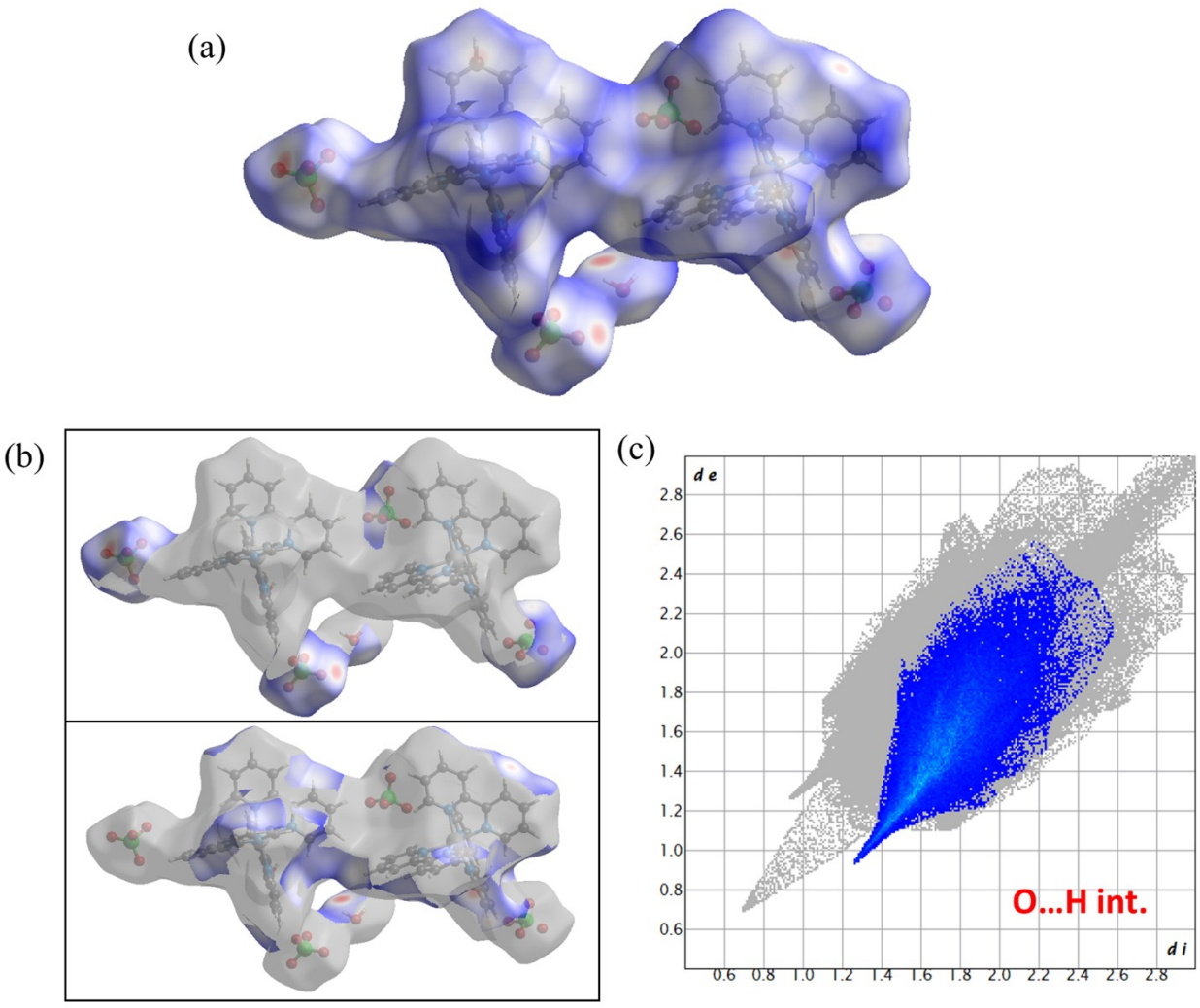

Figure S3. (a) Hirshfeld surface view of **1**, (b) Hirshfeld surface view of inter (upper panel) and intramolecular (lower panel) H-bonding interaction, (c) two-dimensional fingerprint plot of O···H (19.3%) interaction.

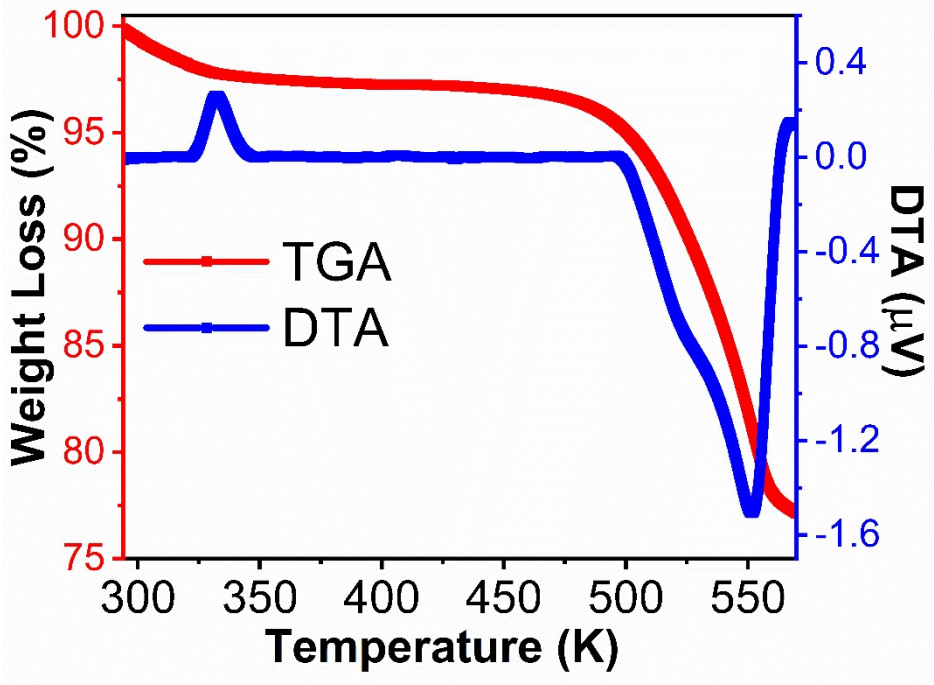

Figure S4. TGA-DTA thermograms of complex **1**.

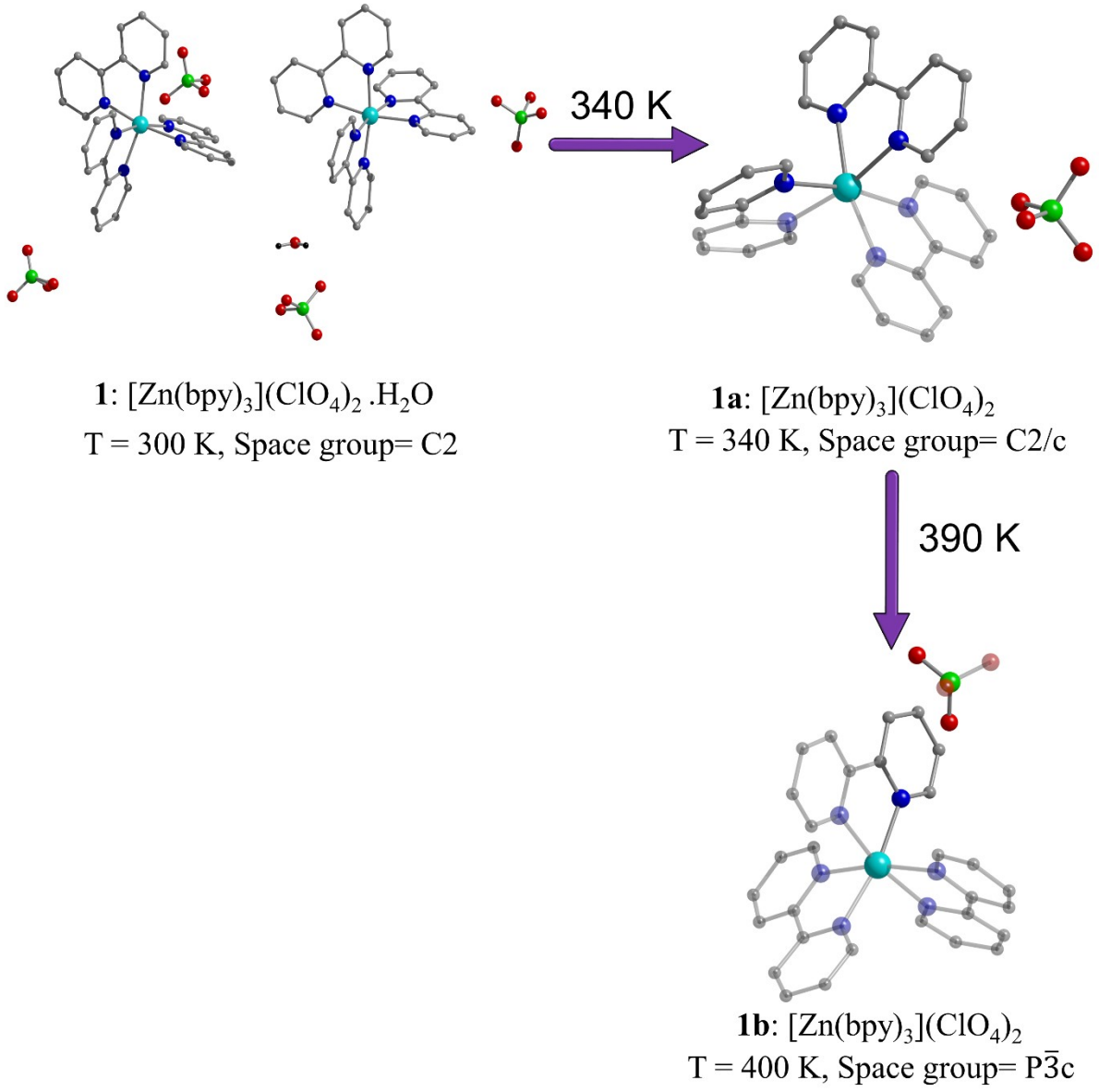

Figure S5. (a) The change in asymmetric unit and irreversible structural transition of **1** to **1a** followed by **1b** with temperature change. Only the asymmetric units are given in solid bonds and the rest of the molecule (symmetry generated part) is shown in transparent bonds.

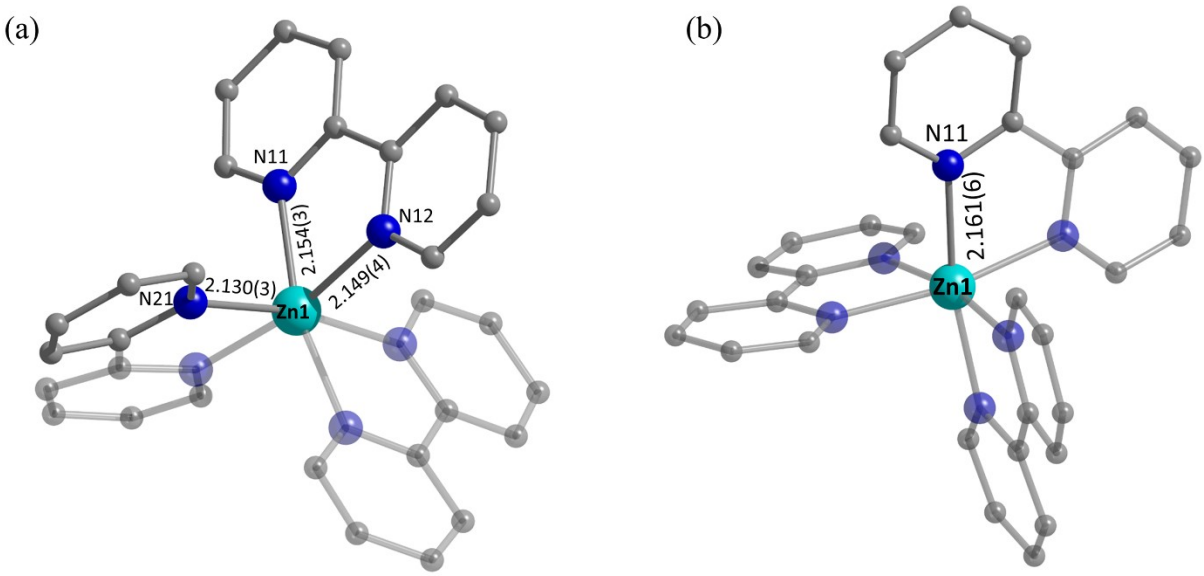

1a: $[Zn(bpy)_3](ClO_4)_2$
T = 340 K, Space group= C2/c

1b: $[Zn(bpy)_3](ClO_4)_2$
T = 400 K, Space group= $P\bar{3}c$

Figure S6. Bond lengths for **1a** and **1b**. Only the asymmetric units (cationic part) are given in solid bonds and the rest of the molecule (symmetry generated part) is shown in transparent bonds.

Table S4: Selected bond angles for complex **1a** (at 340 K)**.**

Bond Angle	**Value (°)**
∠N21[1]-Zn1-N21	76.78(17)
∠N21[1]-Zn1-N11[1]	169.54(13)
∠N21-Zn1-N11[1]	97.79(12)
∠N21[1]-Zn1-N12	95.39(13)
∠N21-Zn1-N12	95.52(13)
∠N11-Zn1-N11[1]	88.91(17)
∠N12[1]-Zn1-N11	94.03(13)
∠N12[1]-Zn1-N11[1]	75.92(13)
∠N12-Zn1-N12[1]	166.07(18)

$1 = -x+1, y, -z+1.5;

Table S5: Selected bond angles for complex **1b** (at 400 K)**.**

Bond Angle	Value (°)
∠N11[1]-Zn1-N11[2]	169.1(3)
∠N11[1]-Zn1-N11[3]	76.3(3)
∠N11-Zn1-N11[3]	92.5(3)
∠N11[1]-Zn1-N11[4]	96.1(2)
∠N11[5]-Zn1-N11[4]	76.3(3)
∠N11[1]-Zn1-N11[5]	92.4(3)

$1 = -x+y-1, -x+1, z; $2= -x, -x+y, -z+1.5; $3 = x+1, -y+1, -z+1.5; $4 = -y+1, x-y+2, z; $5 = x-y+1, -y+2, -z+1.5;

Discussion D1: The increase in temperature results a change in the bond lengths and bond angles of the Zn-N_{bpy} core, ultimately leading to a change in the asymmetric unit and consequently the space group of **1** (Figure S5). At room temperature, the space group of the complex is *C2*, where the asymmetric unit consists of two crystallographically independent molecules. The Zn-N_{bpy} bond lengths are typically in the range of 2.112(9)-2.198(9) Å for both the molecules (Figure S1, *vide supra*). There are also two water molecules present in the asymmetric unit. However, the perchlorate anions and the water molecules were highly disordered, so we masked them during structural refinement. At 340 K, due to the loss of the water molecules, an irreversible structural transition occurs, causing the space group of **1** to change from non-centrosymmetric, monoclinic *C2* to the centrosymmetric, monoclinic *C2/c*. This change gives a new structure **1a** in which the core $[Zn(bpy)_3](ClO_4)_2$ is the same but the asymmetric unit consists of only half of a molecule where the bond lengths are in the range of 2.130(3)-2.154(3) Å (Figure S6a). With more increase in temperature, the space group is further changed to the trigonal, centrosymmetric $P\bar{3}c$, where the asymmetric unit has only half of one bipyridyl moiety attached to the Zn metal and half of the ClO_4^- anion (Figure S6b). The Zn-N_{bpy} bond length is 2.161(6) Å and the bond angles also change accordingly (Tables S1, S4-S5).

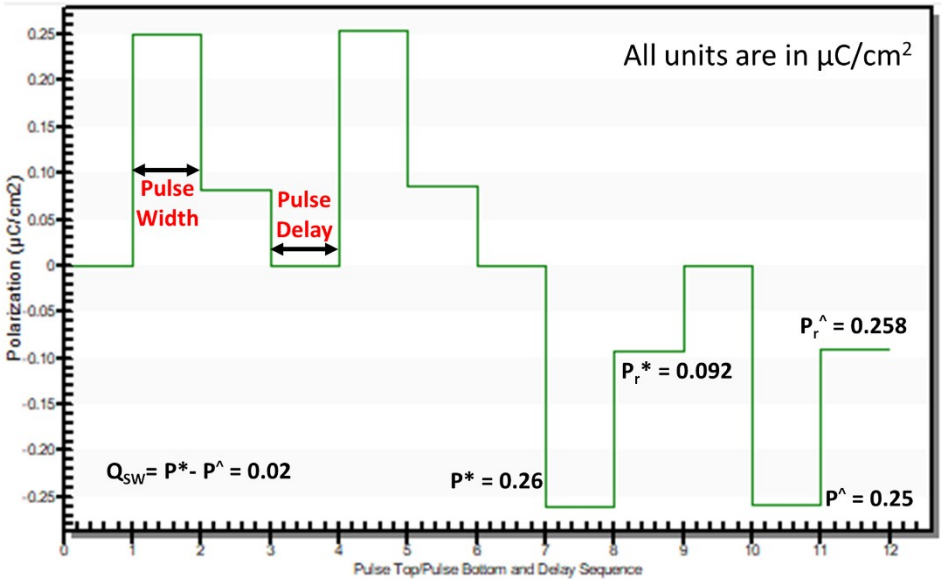

Figure S7. PUND sequence (Positive up and negative down) with a Pulse Width = 1 ms and Pulse Delay = 1000 ms, at 50Hz frequency for **1**.

Figure S8. Domain wall motion behaviour under the act of electric field (+20 V). The phase (φ) images obtained after poling for 4 (a), 8 (b), 12 (c) and 16 (d) minutes. The write dotted square box is chosen to demonstrate how domains are moving from one side to another, evident from yellow vertical lines and red arrows.

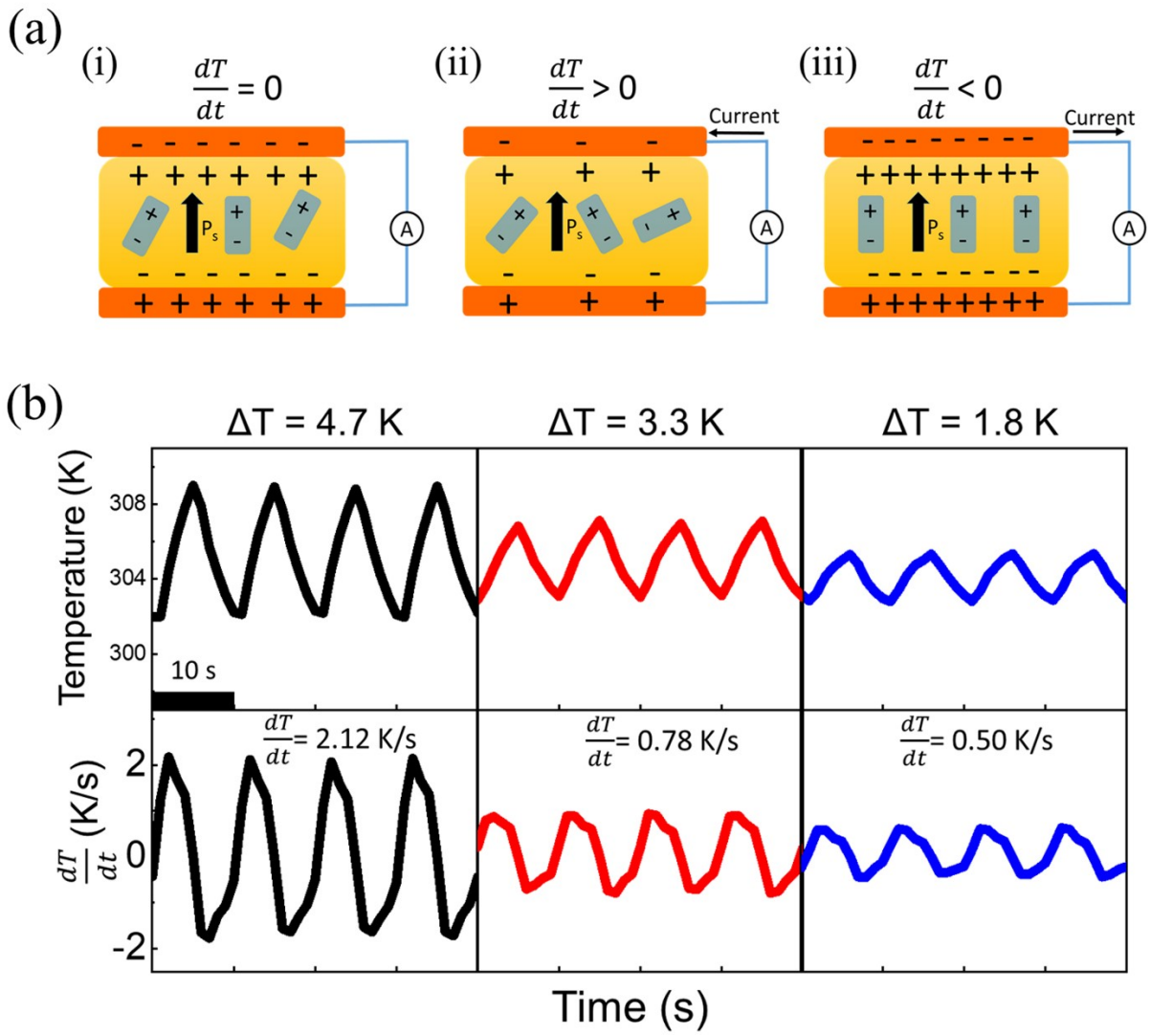

Figure S9. (a) Mechanism of pyroelectric current generation, (b)The input temporal heat profile (upper panel) and its first derivative (rate of change of temperature) employed during pyroelectric current measurement. The corresponding pyroelectric responses from PyG are shown in Figure 4 a (i~iii).